Stanford Exploration Project, Report 112, November 11, 2002, pages 47–65

Velocity estimation for seismic data exhibiting focusing-effect AVO (part 2)

Ioan Vlad[1]

ABSTRACT

Vlad and Biondi (2002) have shown that focusing-effect AVO (FEAVO) exists and is visible in the angle domain. They have conjectured that wave-equation migration velocity analysis (WEMVA) might solve the FEAVO problem. I continue that line of work by showing evidence that WEMVA is the right tool, and by redoing the preprocessing and velocity analysis of the dataset on which FEAVO was defined.

INTRODUCTION

Small velocity anomalies can create AVO effects by focusing the reflected seismic wavefield. This impedes AVO analysis. The AVO anomalies caused by focusing are distinguishable by surface-consistent patterns. Vlad and Biondi (2002) named this phenomenon focusing-effect AVO (FEAVO). In this paper, I present and discuss the feasibility of a method whose application to FEAVO-affected 2D and 3D datasets would produce an estimate of the anomalies. The goal is to determine a velocity field accurate enough to generate a FEAVO-free prestack volume by downward continuing the wavefield through the FEAVO-generating anomalies. The accurate velocity model should be obtained by using the inversion method known as wave equation migration velocity analysis (WEMVA) (Biondi and Sava, 1999), with a fitting goal modified so that it is specifically geared toward extracting FEAVO effects.

I have continued that line of work by going into more depth with regard to each of the aspects of the study. I will respect the same structure. The material presented at each point consists of the progress in knowledge and research accomplished since the previous paper. I begin with a review of previous work used as a basis for my work, then I explain my approach and show evidence of its validity.

PREVIOUS WORK BY OTHERS

Beyond the mere "historical" interest, previous work on defining and describing the FEAVO effect can help answer some potential objections to the proposed approach. For example, one objection might be that FEAVO effects are randomly distributed. Therefore, their expression in

[1]**email:** nick@sep.stanford.edu

AVO pickings is the same as that of random noise, and can be treated the same way. White et al. (1988) showed that focusing and defocusing caused by a random distribution of small velocity anomalies will not lead to the canceling of the FEAVO effects by each other. Moreover, they prove that even if the distribution of velocity anomalies is random, the probability that FEAVO effects appear is not randomly distributed with the distance from the shot. Therefore, FEAVO presence cannot be equated with random noise in AVO picking, since FEAVO-causing anomalies are not randomly distributed in real data. In the case of shallow anomalies the distribution is influenced by depositional patterns [the "Rotten alligators" in Claerbout (1985)], and in the case of deep-origin FEAVO, by the presence of faults (Hatchell, 2000). Besides, the amplitude of the FEAVO effects is often so large and spatially extended that it renders AVO analysis impossible.

Attempts to invert FEAVO-affected data for a velocity model

The main papers discussing aspects of solving the FEAVO problem are Kjartansson (1979), Woodward (1987), Claerbout (1993), Bevc (1994), and Harlan (1994). All are iterative inversions that try to find the velocity model that will result in the given raw data. With the exception of Harlan (1994), this operator is some form of plane-wave decomposition using a straight-ray assumption; none uses an actual differential ("wave-equation") operator. Woodward (1987) applies corrections in order to account for differences between infinite-frequency rays and the "fat rays" associated with the physics of wave propagation. All of them, with the exception of Harlan (1994), invert either for the traveltime effects associated with AVO, or for the amplitudes, but not for both simultaneously.

None of the previous attempts is completely successful in producing a velocity model that satisfies the initial goals of the problem. Using only a two-dimensional midpoint-offset map of FEAVO effects, instead of recognizing that they correlate across depth (as equation 3 and Figure 9 show), they introduced too many degrees of freedom in the inversions. Considering only straight rays was incorrect even in the case of the universally encountered v(z) variation. All methods require some form of picking, which results in endless headaches. None makes successful use of the entire quantity of information by simultaneously considering both the traveltimes and the amplitudes for all the reflectors. Only one (Harlan, 1994) incorporates the information given by standard velocity analysis (which is not significantly affected by FEAVO effects).

Wave Equation Migration Velocity Analysis

Like tomography, migration velocity analysis (MVA) is a velocity analysis method by iterative inversion. The difference between the two is at a "strategic" level: instead of trying to find the velocity model that will result in the given raw data, it tries to find the velocity through which prestack migrated data results in a perfectly focused image. The chapter pertaining to velocity analysis in Biondi (2001) shows why dipping reflectors in laterally varying velocity media require the velocity analysis to be performed in the migrated domain (image domain) instead of the unmigrated domain (data domain).

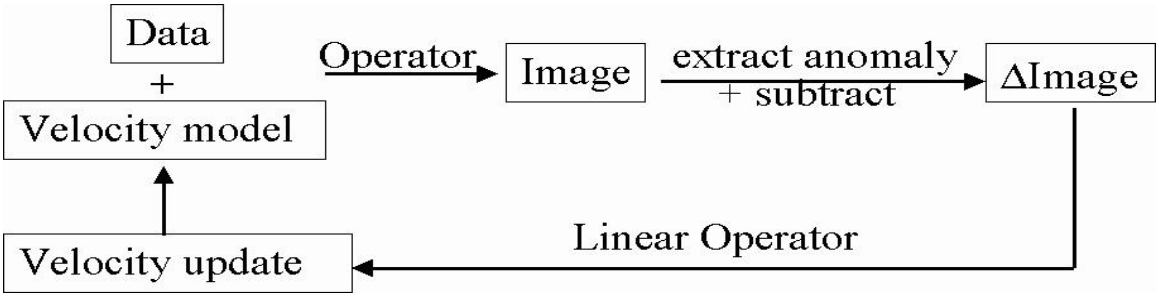

Figure 1: Migration Velocity Analysis flowchart nick2-invpic [NR]

MVA can be done with infinite-frequency (ray-based) operators (Clapp, 2001) or with finite band (wave-equation) operators (Biondi and Sava, 1999). The advantages of the latter over the former are detailed in the WEMVA chapter of Biondi (2001). In particular, ray theory breaks down if its high frequency assumption does not hold (Woodward, 1990), as is the case with velocity anomalies of the size of those that generate the FEAVO effect. Multipathing is another instance when the wave equation methods are more appropriate. They also treat more correctly the amplitudes.

WEMVA proceeds as follows: the wavefield at a certain depth is downward continued a depth step through the known velocity model with an accurate (nonlinear) operator. The result is transformed to angle domain and an improved image is created by eliminating either the curvature of the events in angle-domain common image gathers[2] (Prucha et al., 1999), or the FEAVO anomalies. An image perturbation (ΔImage) is obtained by subtracting the two images, and is backprojected through an invertible operator in order to obtain a velocity update. The velocity model is updated and the cycle proceeds again until ΔImage becomes negligible. Figure 1 illustrates this process.

WEMVA is at the forefront of research. As the comparison in the next section will show, it avoids all the shortcomings of the previous attempts.

THE NEW APPROACH

My goal is to modify a brand-new tool (WEMVA) to the specific of an old unsolved problem (velocity model finding for FEAVO elimination). The FEAVO anomalies will be eliminated by finding an accurate velocity model, then by downward continuing the data through it After obtaining a velocity model good enough to help eliminate the FEAVO, the significance of the process will be tested by performing geological interpretations of the data with and without the FEAVO anomalies.

The strategy of WEMVA differs from that of all the previous attempts: instead of trying to fit the data, it tries to fit the image. The tactics are different as well: instead of integral (ray-based, Kirchhoff) operators, it uses differential (wave-equation) ones, with all their well-

[2]referred from now on simply as “angle gathers,” or by the acronym ADCIGs

known advantages. Unlike most of the previous approaches, this one is capable of using a starting guess from classic velocity analysis. Therefore, it simply fine tunes the velocity model for small velocity anomalies. It requires no picking and tries to match the entire image using information contained both in the amplitudes and traveltimes.

This new approach, unlike the old ones, takes into account all the characteristics of the FEAVO anomalies, including the variation with depth. This goal is achieved by measuring anomalies on surfaces in the depth-midpoint-angle volume, instead of simple "V"s in the midpoint-offset plane. An adaptation of the signal-noise separation technique described in Harlan (1986) will assure that the image perturbation contains only information related to the FEAVO anomalies.

My approach uses the strategy and framework of WEMVA as described in the corresponding section, but differs by the change of objective function in the inversion. The usual WEMVA criterion describing the quality of the image is flatness in angle gathers that is directly related to traveltime anomalies. The traveltime changes associated with the FEAVO effect are very small and do not produce whole-event curvature, but only wiggliness in angle gathers. Biondi and Sava (1999) show on a synthetic, and this paper will show on a real dataset, that FEAVO anomalies keep their "V" shapes through prestack migration and conversion from offset to angle gathers. Therefore, the fitting goal of the inversion must be related to the distribution of amplitudes in the midpoint-angle space. The desired image will not exhibit the characteristic "V" patterns in the midpoint-offset plane.

My method might be able to discriminate between amplitude anomalies caused by absorption and those caused by velocity because both kinds of anomalies have two different "signatures" in the image space. In the case of velocity, the high amplitudes are found close to the low amplitudes: the energy is not lost but it is only focused locally. In the case of absorption the FEAVO effects are not "bipolar."

EVIDENCE THAT THE PROPOSED APPROACH IS FEASIBLE

As stated by Vlad and Biondi (2002), the heuristic for proving that the inversion approach is feasible comprises three steps:

1. Proving that shallow-origin FEAVO anomalies are visible in the angle domain and wave-equation methods correctly handle the deep-origin FEAVO effects in synthetic data. That was first accomplished by Vlad and Biondi (2002) and in this paper I present some improved results.

2. Proving that the anomalies can be extracted in the angle domain. I will show that in the case of simple velocity distributions, the shape of the anomalies is described by very simple analytical formulas and I will discuss ways to extract them.

3. Proving that the extracted anomalies can be transformed back to the initial domain, updating the guess. In particular, that the linearized downward continuation does not render FEAVO effects unrecognizable.

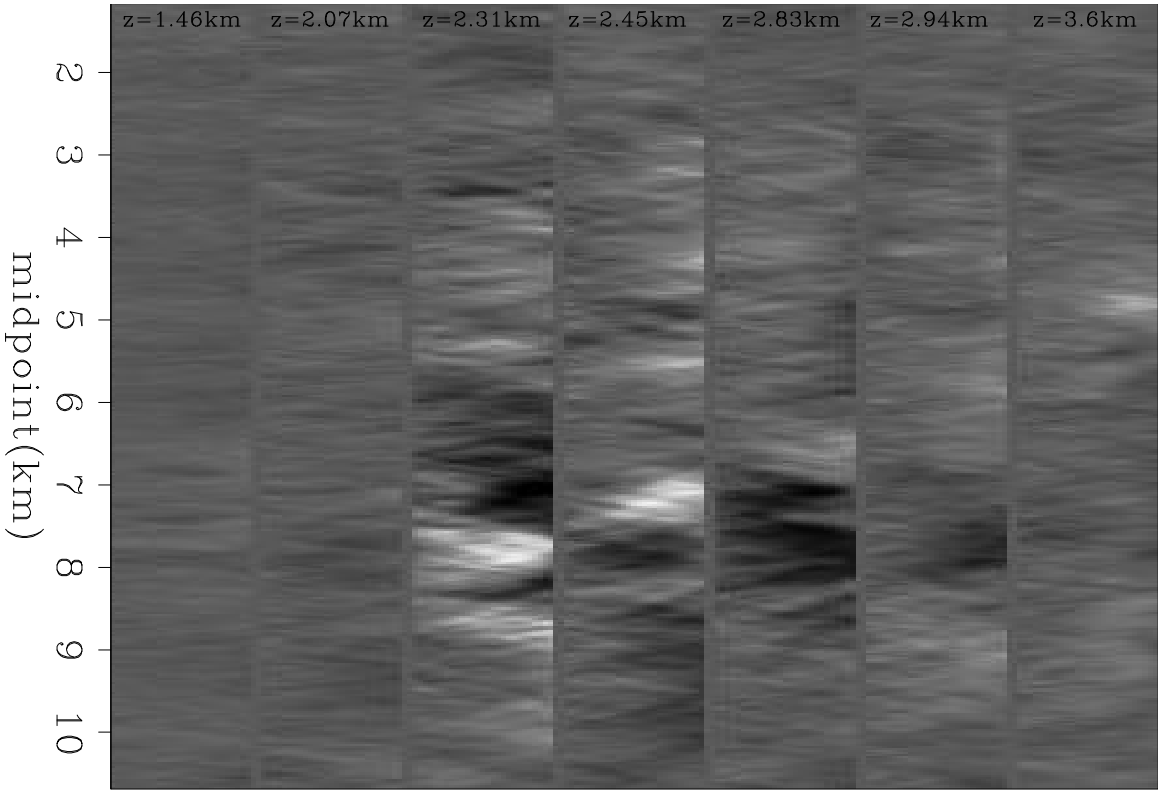

Figure 2: Midpoint-angle slices, reprocessed dataset, new velocity analysis. The improvement in quality allowed the panels to go up to 25 degrees, instead of only 20 in the previous paper. nick2-fkapanel [CR]

Shallow-origin FEAVO effects

Vlad and Biondi (2002) have proven this point using the very dataset on which FEAVO was first observed by Kjartansson (1979); however, its preprocessing and preliminary velocity analysis left a lot of room for improvement. The details of the preprocessing are described and illustrated in Appendix C. A new velocity analysis, also illustrated in Appendix C, follows. The result of phase-shift migration and conversion to angle gathers is visible in Figure 2.

Deep-origin FEAVO effects

Hatchell (2000) proves using both real and synthetic data that FEAVO effects can be generated not only by shallow velocity anomalies, but also by deep ones. They usually have a different origin than the shallow ones. They appear not because of depositional irregularities, but because of sudden terminations of thin layers with anomalous velocity against subvertical faults. The question of whether the deep-origin FEAVO behaves like its shallow counterpart and are visible in angle gathers is, therefore, legitimate.

The easiest way to answer this would be to repeat the same experiment as in the previous

subsection, but real data containing deep-origin FEAVO is not yet available. Therefore, I will use synthetic data to show that wave-equation methods handle well the deep-origin FEAVO effects. These results are in Appendix A.

Extracting FEAVO effects in angle gathers

Extracting the FEAVO anomalies assumes that the long spatial wavelength velocity model is good enough that the reflectors are flat in angle gathers, and only the amplitudes remain to be fixed. Since the FEAVO effects are expressed both in the midpoint-angle domain and in the angle-domain common image gathers, their separation must proceed in a synergistic fashion. This involves the entire data volume. For the simplest case (constant velocity, flat reflectors), the FEAVO effects generated by a velocity anomaly at depth z_a and midpoint m_a will be distributed in the depth(z)–midpoint(m)–angle(θ) space along a surface described by:

$$z = z_a + |m - m_a| \cot\theta. \tag{1}$$

The derivation is laid out in Appendix B, and the shape of the surface is shown in Figure 3. Even for a v(z) case (Grand Isle dataset), the shape of the anomaly will not be very different,

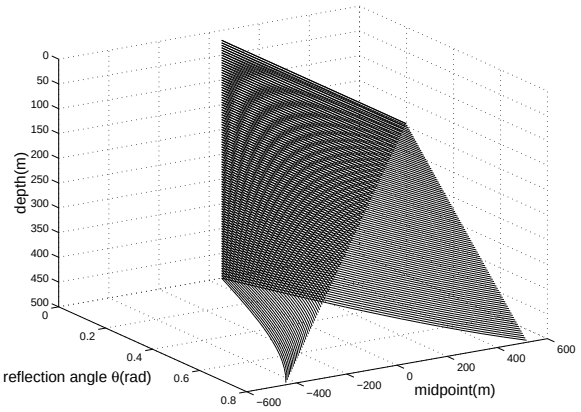

Figure 3: Shape of the FEAVO "footprint" in the depth-midpoint-angle space due to a velocity anomaly 20 m deep in an otherwise constant velocity medium with flat reflectors. For a better 3D visual understanding, the shape resembles the bow of a flipped boat. nick2-ang3d_20_500_pi4 [NR]

especially for a limited angle range (due to a finite range of offsets). Figure 4 shows the dips of the FEAVO effects are confined to a limited range. Therefore, as a first measure for separating them, we can apply an appropriate f-k dip filter to the midpoint–angle slices (Figure 2). This eliminates the largest part of the petrophysical AVO. There is, however, no guarantee that the remaining energy within the plausible FEAVO dip range does actually belong to FEAVO. I will have to separate the signal from noise in the manner of Harlan (1986):

1. For each point in the depth-midpoint section, consider that it "houses" an anomaly and precompute the FEAVO-effect surface that depends on the known long spatial wavelength velocity field.

2. Sum (or compute a semblance-like operator) along the precomputed surfaces to obtain a depth-midpoint "anomaly map," taking care to distinguish between FEAVO caused by absorption and that caused by velocity.

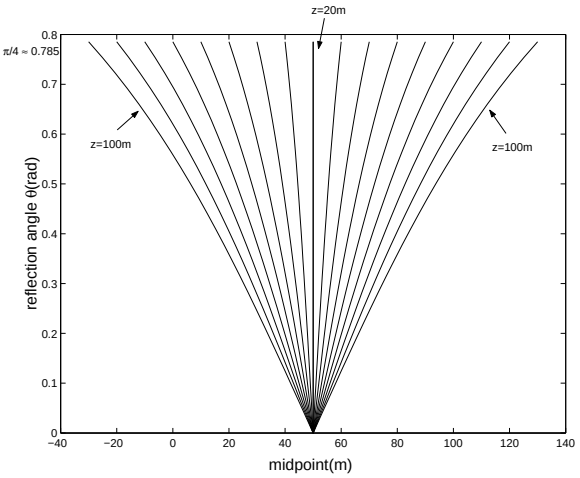

Figure 4: Midpoint–angle contour map of FEAVO effects generated by a velocity anomaly 20m deep. The angle range is wide (up to 45°), which is wider than the range recorded in most of the real data sets. Therefore, it is unlikely that curvature of the anomalies be observed in real data panels. nick2-ang20_100_pi4 [NR]

3. Filter the image based on its statistical properties, so only the most focused points remain.

4. Spread the filtered image along the precomputed surfaces back into the depth-midpoint-angle space. Alternately, focusing could be done using the downward continuation operator itself.

Linearized downward continuation preserves the FEAVO effects

The third WEMVA step relies on inverting a linearized downward continuation operator in order to obtain the velocity perturbation from the image perturbation. This means the linearization must not destroy the FEAVO anomalies. One way to check this is to actually do WEMVA for a synthetic case. A smarter, less time-consuming way is to see whether the non-inverted operator correctly propagates a wavefield through a velocity anomaly to create a FEAVO effect.

A good comparison case can be provided by the waveform modeling of deep FEAVO anomalies (Figure 6). Figure 5 represents the results of an equivalent experiment - propagating a shot (20Hz Ricker wavelet, laterally smoothed a bit) from the surface to a line of receivers 6 km deep. The difference is that in Figure 5 the propagation was done with linearized downward continuation [the complexified local Born-Fourier method (de Hoop et al., 2000), as described by Sava (2000)], instead of pseudospectral waveform modeling. Details about the operator and the way the image was constructed are in Appendix B. The FEAVO effects are easily recognizable in amplitudes and the dispersion is missing. Even if they are less powerful than in Figure 6, especially in time, they are clearly distinguishable.

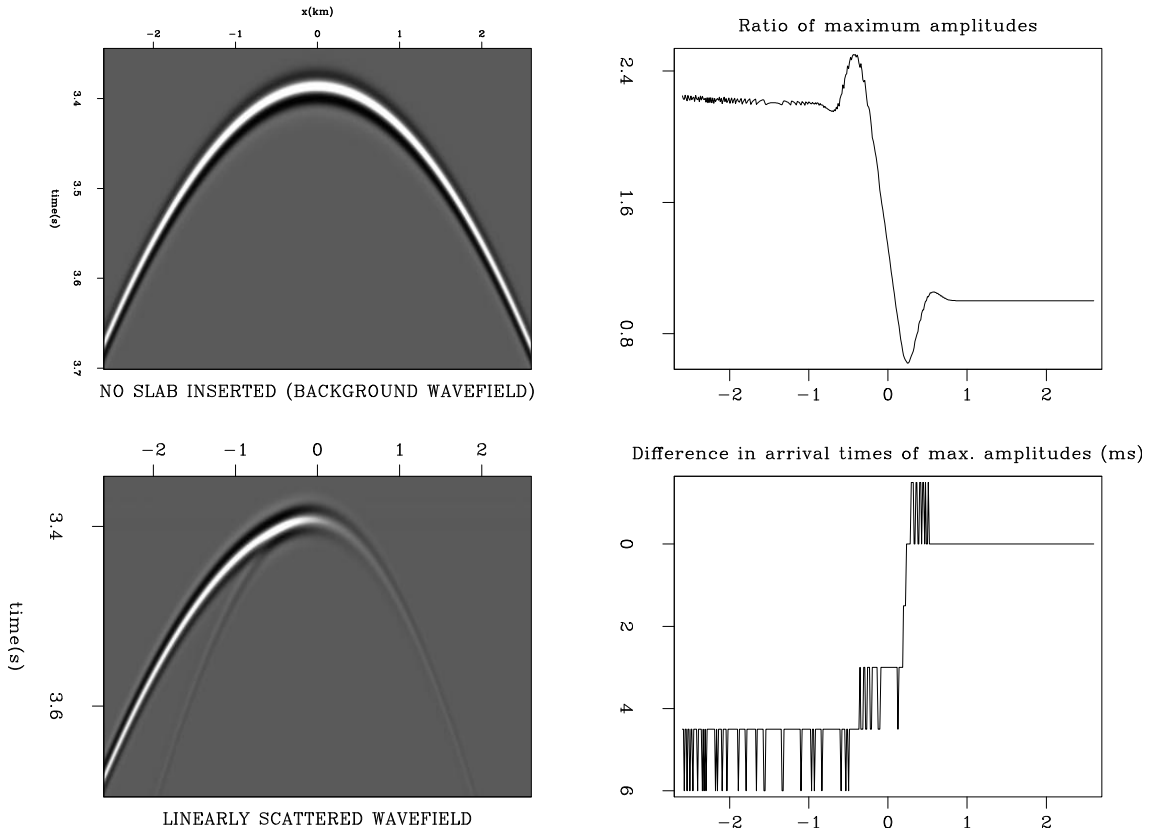

Figure 5: **Left, from top to bottom:** 1. Wavefield recorded 6 km deep after propagation through constant velocity (background wavefield); 2. Linearly scattered wavefield (physically equivalent to the difference between the wavefield propagated through the velocity model containing the slab – panel 6 of Figure 6 – and the background wavefield); **Right, from top to bottom:** 3. Ratio between the maximum amplitudes in panel (1+2) and panel 1, for each x location; 4. Difference between the times of the maximum amplitudes in 1 and (1+2), for each x location. The wavefield was propagated by linearized downward continuation (complexified local Born-Fourier method) instead of pseudospectral waveform modeling. nick2-popic [CR]

CONCLUSIONS

Building a velocity model accurate enough to remove FEAVO effects by prestack depth migration is an important problem which has not been solved satisfactorily until now. WEMVA, with a fitting goal adapted to the specific morphology of the anomalies, is a promising tool that will likely solve the problem. Work in this direction has proven that the iterative inversion is feasible: real data focusing effects are visible in the angle domain, the anomalies are preserved by waveform modeling, and the linearized downward continuation operator does not destroy the anomalies.

FUTURE WORK

The previous sections have proven that an inversion for the velocity model that produces the FEAVO anomalies is possible. The actual work of setting up such an inversion first for 2D, then for 3D, remains to be done. While the functioning of the forward and the inverse operators for the iterative inversion is being proved by the work of Paul Sava, I have to replace his approach of constructing $\Delta Image$ with my approach of extracting the FEAVO anomalies.

I will also need to investigate ways to discriminate between absorption and velocity caused FEAVO. I plan to study the effects of the source directivity on the amplitudes and to investigate a non-smoothing styling goal for the inversion. I would have to investigate ways to do surface-consistent amplitude corrections that will account for surface absorption variations, and to see whether that will not destroy the FEAVO.

Finally, I will perform geological interpretations of the data with FEAVO removed, and compare them with interpretations of the original data. This should show that FEAVO removal and the new velocity model made a difference in interpretation results.

ACKNOWLEDGMENTS

I am grateful to Biondo Biondi for providing me strategic guidance pertaining to the approach to the problem and for the waveform modeling in Figure 6, to Paul Sava and Bob Clapp for their constant good advice and support, and to Rick Ottolini and Andrey Karpushin for bringing relevant references to my attention.

REFERENCES

Bevc, D., 1994, Datuming velocity from traveltime tomography: SEP–**82**, 145–164.

Biondi, B., and Sava, P., 1999, Wave-equation migration velocity analysis: SEP–**100**, 11–34.

Biondi, B. 3-d Seismic Imaging:. http://sepwww.stanford.edu/sep/biondo/Lectures, 2001.

Claerbout, J. F., 1985, Imaging the Earth's Interior: Blackwell Scientific Publications.

Claerbout, J. F., 1993, Reflection tomography: Kjartansson revisited: SEP–**79**, 59–68.

Clapp, R. G., Sava, P., and Claerbout, J. F., 1998, Interval velocity estimation with a null-space: SEP–**97**, 147–156.

Clapp, R. G., 2001, Geologically constrained migration velocity analysis: Ph.D. thesis, Stanford University.

de Hoop, M. V., le Rousseau, J. H., and Wu, R.-S., 2000, Generalization of the phase-screen approximation for the scattering of acoustic waves: Wave Motion, **31**, no. 1, 43–70.

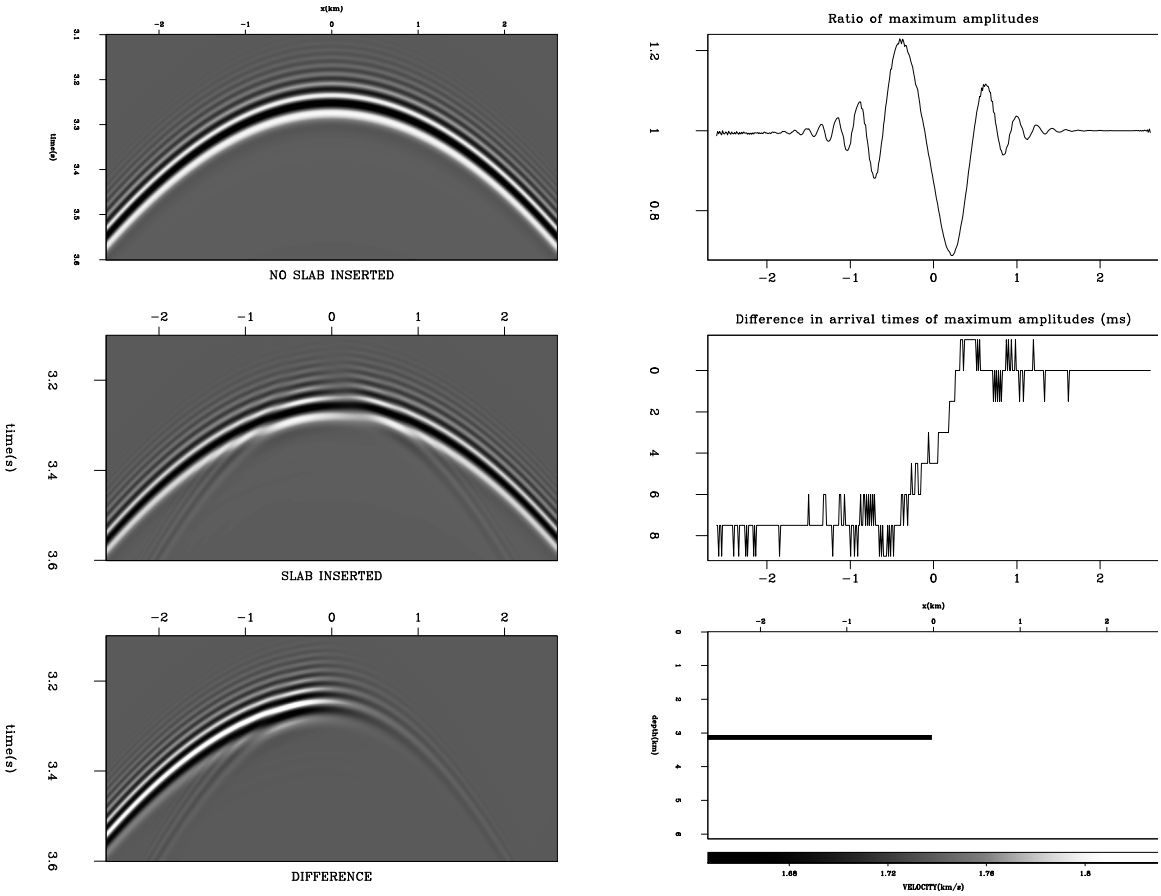

Figure 6: **Left, from top to bottom:** 1. Wavefield recorded 6 km deep after propagation through constant velocity; 2. Wavefield recorded 6 km deep after propagation through velocity model in panel 6; 3. Difference between 1 and 2; **Right, from top to bottom:** 4. Ratio between the maximum amplitudes in panel 2 and panel 1, for each x location; 5. Difference between the times of the maximum amplitudes in 1 and 2, for each x location; 6. Velocity model for panel 2 – homogeneous with a lower velocity slab inserted. nick2-hatsim [CR]

Harlan, W. S., 1986, Signal-noise separation and seismic inversion: Ph.D. thesis, Stanford University.

Harlan, W. S., 1994, Tomographic correction of transmission distortions in reflected seismic amplitudes: 64th Annual Internat. Mtg., Soc. Expl. Geophys., Expanded Abstracts, 968–971.

Hatchell, P., 2000, Fault whispers: Transmission distortions on prestack seismic reflection data: Geophysics, **65**, no. 2, 377–389.

Kjartansson, E., 1979, Analysis of variations in amplitudes and traveltimes with offset and midpoint: SEP–**20**, 1–24.

Ottolini, R., and Rocca, F., 1982, Direct observation of lateral velocity anomalies in field data: SEP–**32**, 15–23.

Prucha, M., Biondi, B., and Symes, W., 1999, Angle-domain common-image gathers by wave-equation migration: 69th Ann. Internat. Meeting, Soc. Expl. Geophys., Expanded Abstracts, 824–827.

Sava, P., 2000, A tutorial on mixed-domain wave-equation migration and migration velocity analysis: SEP–**105**, 139–156.

Vlad, I., and Biondi, B., 2002, Velocity estimation for seismic data exhibiting focusing-effect avo: SEP–**111**, 107–123.

White, B. S., Nair, B., and Bayliss, A., 1988, Random rays and seismic amplitude anomalies: Geophysics, **53**, no. 07, 903–907.

Woodward, M., 1987, Reflection tomography : Vees in midpoint offset space: SEP–**51**, 1–12.

Woodward, M., 1990, Wave equation tomography: Ph.D. thesis, Stanford University.

APPENDIX A – DERIVATION OF FORMULAS FOR FEAVO ANOMALY SHAPES

All the derivations that follow are made under the assumption that the velocity is constant (straight rays) and that all reflectors are flat and horizontal. In order to derive the shape of FEAVO effects in the angle domain (1), we first derive the shape of FEAVO effects in the offset domain. Consider case B (the general case) in Figure 7 Vlad and Biondi (2002). For the zero-offset experiment, the focusing-generating anomaly affects only its own midpoint. For any other offsets, it affects two midpoints that grow increasingly distant with offset. In Figure 8, because the reflector is parallel to the surface,

$$\left.\begin{array}{c} CD||AE \Rightarrow B\hat{D}C = D\hat{A}E \\ DCB = AED = 90^\circ \end{array}\right\} \Rightarrow \Delta BDC \approx \Delta DAE \Rightarrow \frac{BC}{DE} = \frac{DC}{AE} \Rightarrow \frac{z - z_a}{z} = \frac{m - m_a}{f/2} \tag{2}$$

Applying the same reasoning to the left side of case B in Figure 7, we can write the equation for both slanted streaks at depth z as

$$f = \frac{z}{z - z_a} \cdot 2\,|m - m_a| \tag{3}$$

Figure 9 depicts parts of the corresponding surface for a 20m deep anomaly. Notice the arched form of the surface with the midpoint–depth vertical planes at maximum offset. This (with very different vertical scaling) is the "bullet shape" observed by Ottolini and Rocca (1982) in a real dataset. The offset f can be easily replaced with the reflection angle in this case because the reflector is flat:

$$\theta = A\hat{D}E \Rightarrow \tan\theta = \frac{AE}{ED} = \frac{f}{2z}. \tag{4}$$

Plugging in (3),

$$|m - m_a| = (z - z_a)\tan\theta \tag{5}$$

which can also be written as (1).

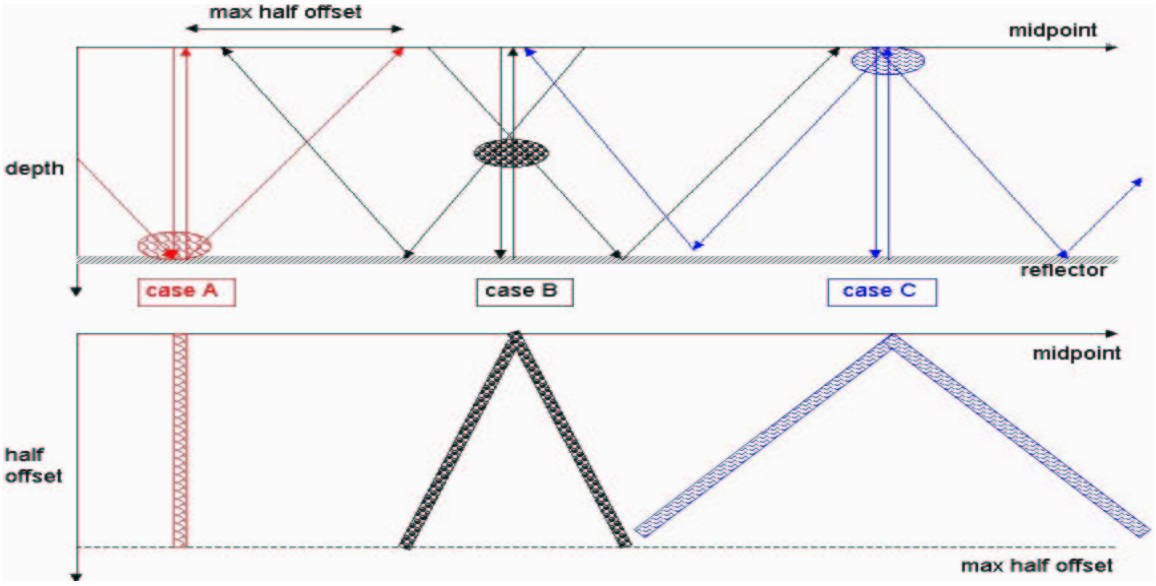

Figure 7: Physical explanation for the expression of FEAVO anomalies in midpoint-offset space. In the upper picture, the blobs are transmission anomalies and the arrows are raypaths for zero offset and maximum offset recordings. For case A (anomaly on the reflector), only a single midpoint is affected for all offsets. Case C (anomaly at the surface) is actually a static: its "footprint" is a pair of streaks slanting 45^o from the offset axis. Case B (in between) gives a pair of streaks with angles smaller than 45^o. nick2-vilus [NR]

APPENDIX B – THE FORWARD LINEARIZED DOWNWARD CONTINUATION OPERATOR

Downward continuation can be done in the Fourier domain as a phase shift applied to U_z, the wavefield at depth z (Claerbout, 1985):

$$U_{z+\Delta z} = e^{ik_z \Delta z} U_z \tag{6}$$

The vertical wavenumber k_z depends on the laterally varying velocity. In order for us to be able to implement the formula, we have to decompose k_z into a part not influenced by lateral velocity variations (k_{z_o}) and a part influenced by them (k_{z_x}):

$$k_z = k_{z_o} + k_{z_x} \Rightarrow U_{z+\Delta z} = e^{i(k_{z_o}+k_{z_x})\Delta z} U_z \Rightarrow U_{z+\Delta z} = e^{ik_{z_o}\Delta z} e^{ik_{z_x}\Delta z} U_z \tag{7}$$

The Born approximation is equivalent to a linearization of the exponential $e^x \approx 1 + x$, and therefore

$$U_{z+\Delta z} \approx e^{ik_{z_o}\Delta z} U_z (1 + ik_{z_x}\Delta z) \tag{8}$$

In the case of the complexified local Born-Fourier (complexified pseudo-screen) method, with the notations in equations (12) and (13) of Sava (2000), we can rewrite it as:

$$U_{z+\Delta z} \approx \mathcal{T} U_z [1 + \mathcal{S}(s - s_o)] \tag{9}$$

where $\mathcal{T}$ is the background wavefield downward continuation operator applied in the $\omega - \mathbf{k_m}$ domain:

$$\mathcal{T} = e^{i\,\Delta z \sqrt{\omega^2 {s_o}^2 - (1-i\eta)^2 |\mathbf{k_m}|^2}}, \tag{10}$$

$\mathcal{S}$ is the scattering operator, applied in the $\omega - x$ domain:

$$\mathcal{S} = \frac{i\,\Delta z \omega^2 s_o}{\sqrt{\omega^2 {s_o}^2 - (1-i\eta)^2 |\mathbf{k_m}|^2}} \tag{11}$$

and where s is the slowness at the depth $z + \Delta z$, $\mathbf{k_m}$ is the wavenumber across the midpoint direction (scalar for 2D, vector for 3D), s_o is the constant background slowness, ω is the frequency, and η is a small dimensionless quantity introduced for numerical stability; $\mathbf{k_m}$ and ω must contain a 2π constant. The output of this operator can be seen in Figure 10.

Although with equation (9) we went a step towards linearity with respect to the slowness perturbation term, it is not fully linear because the slowness perturbations compose with themselves. This is visible if we examine the first two steps of the downward continuation. At $z = 0$, $U_{z=0} = Data$ (Ricker wavelet at zero-time in the middle of the x axis). At $z = \Delta z$,

$$U_{z=\Delta z} = \mathcal{T} U_{z=0} + \mathcal{S} \Delta s_{z=\Delta z} \mathcal{T} U_{z=0}. \tag{12}$$

At $z = 2\Delta z$,

$$U_{z=2\Delta z} = \mathcal{T} U_{z=\Delta z} + \mathcal{S} \Delta s_{z=\Delta z} \mathcal{T} U_{z=\Delta z}, \tag{13}$$

and by plugging in the expression for $U_{z=\Delta z}$ and because $\mathcal{T}$ and $\mathcal{S}$ do not commute,

$$U_{z=2\Delta z} = \mathcal{T}\mathcal{T} U_{z=0} + \mathcal{T}\mathcal{S}\Delta s_{z=\Delta z}\mathcal{T} U_{z=0} + \mathcal{S}\Delta s_{z=2\Delta z}\mathcal{T}\mathcal{T} U_{z=0} + \mathcal{S}\Delta s_{z=\Delta z}\mathcal{T}\mathcal{S}\Delta s_{z=2\Delta z}\mathcal{T} U_{z=0} \tag{14}$$

In order to obtain a downward continuation that is linear in the slowness perturbations Δs, we have to drop the last term at each step. Thus, after the n^{th} depth step, the wavefield will be:

$$U_{z=n\Delta z} = \left(\prod_1^n \mathcal{T}\right) U_{z=0} + \sum_{j=1}^{n} \left[\left(\prod_1^{n-j} \mathcal{T}\right) \mathcal{S}\Delta s_{z=j\Delta z} \left(\prod_1^{j} \mathcal{T}\right) U_{z=0} \right] \tag{15}$$

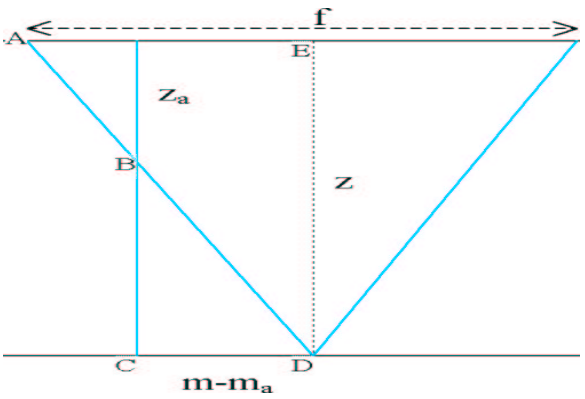

Figure 8: The right half of case B in Figure 7. Raypaths are in blue. The transmission anomaly is in B, at a depth of z_a. AE (of length f – full offset) is at the Earth's surface, C is on the reflector at the anomaly midpoint (m_a), D is on the reflector at midpoint m and depth z. DE is perpendicular to the surface; BC is perpendicular to the reflector. nick2-skema2 [NR]

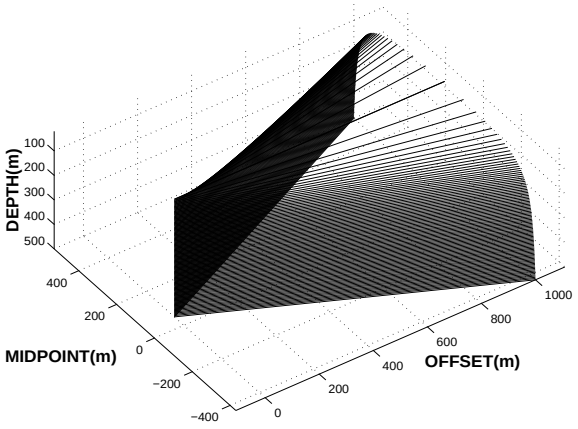

Figure 9: Fragment of the surface described by equation 3, between 0 and 500m, for a transmission anomaly 20 m deep. The shape resembles the bow of an overturned boat. nick2-20_max500 [NR]

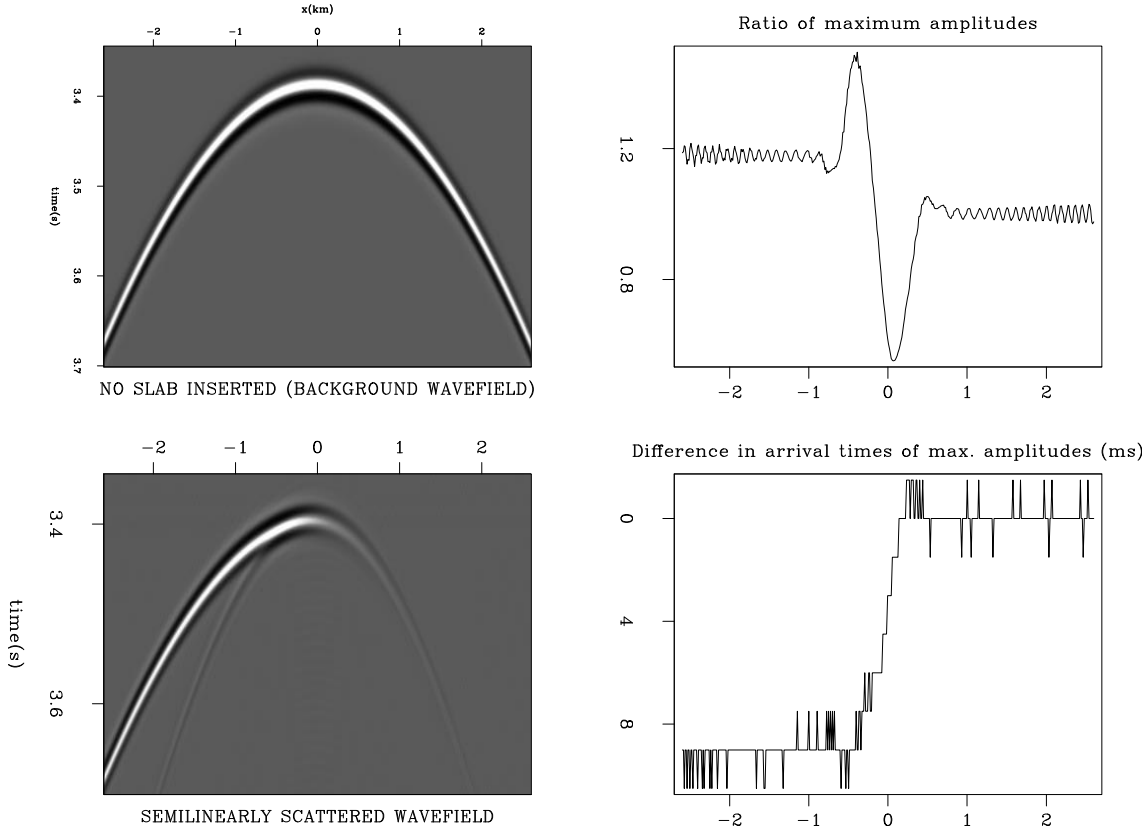

Figure 10: **Left, from top to bottom:** 1. Wavefield recorded 6 km deep after propagation through constant velocity (background wavefield); 2. Quasi linearly scattered wavefield (physically equivalent to the difference between the wavefield propagated through the velocity model containing the slab – panel 6 of Figure 6 – and the background wavefield); **Right, from top to bottom:** 3. Ratio between the maximum amplitudes in panel (1+2) and panel 1, for each x location; 4. Difference between the times of the maximum amplitudes in 1 and (1+2), for each x location. The wavefield was propagated with the operator in equation 9. Panel 4 is in very good accord with panel 4 of Figure 6 and with the analytical time delay (8.7 ms). nick2-patpic [CR]

The above formula is equivalent with stating that at each level, we compute the scattered wavefield only from the background wavefield from the previous level, then we propagate it down until the last level with the background operator. The results of this approach are visible in Figure 5.

APPENDIX C - PREPROCESSING DETAILS

I first applied better tuned f-k filters, then shifted the data 9 meters across offset using a frequency-domain operator. Why? The migration program `Phase` requires data to be regularly sampled to contain the zero offset. The minimum offset of the data was 241m and the offset sampling was 50m (interpolated to 25), so there was no way of having both the zero offset and regularly sampled data. Worse, `Phase` requires split-spread data, so half of the offsets would have been off by 9 meters. I then performed f-x decon to eliminate random noise. I interpolated the offsets from a sampling rate of 50m (visible aliasing) to 25m in the wavenumber domain. I performed deconvolution using `Pef` and `Helicon`. I had to apply again f-k filters with new parameters to eliminate some of the effects of former aliasing, which turned into spurious events after interpolation.

Figures 11 and 12 show the smallest non-extrapolated offset before and after the new preprocessing, respectively. The railroad-track reflections above 1.5 seconds, which is actually water-velocity noise, is eliminated and the geology beneath is uncovered (due to the dip filters). The strong ringing which multiplied reflectors most visibly in the high-amplitude region is gone (due to deconvolution). The signal/noise ratio between 3 and 5 seconds is highly improved (due to the f-x decon). After the new preprocessing, the stratigraphy looks much more interpretable and new, subtler FEAVO anomalies are brought to light. The V-shaped anomalies were not destroyed; on the contrary, they are clearer than ever (Figure 13).

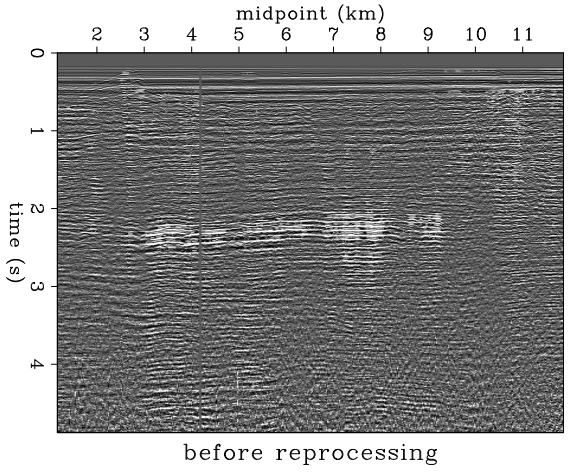

Figure 11: Smallest offset (241m) before reprocessing nick2-zofbef [CR]

The previous velocity model, which is already existing in the data library, is shown in the upper left panel of Figure 14. The geological setting of the Grand Isle survey in the Mississippi Delta shows that the Grand Isle deposits are very young and the velocity is most likely

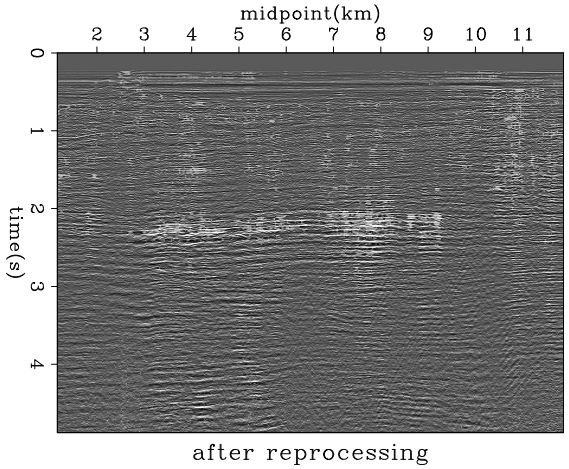

Figure 12: Smallest offset (250m) after reprocessing. Railroad-track false reflections above 1.5 sec, ringing all over the section and high noise in the lower part are eliminated. nick2-zofaft [CR]

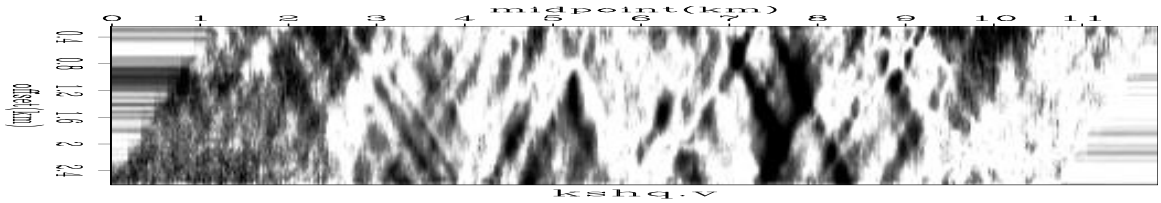

Figure 13: Preprocessing enhanced the V-shaped anomalies nick2-kshq [CR]

determined by compaction, making such large lateral velocity variations as pictured in the initial model implausible. The previous velocity had also been picked at only ten midpoints.

I eliminated random noise from the data with an enhanced noise attenuation method. I then transformed each CMP to velocity space, automatically picked the highest semblance values, and transformed them to interval velocity using the "SuperDix" inversion described by Clapp et al. (1998) (Figure 15). The result of the inversion was then smoothed along midpoint into a more geologically plausible almost-v(z).

I migrated with the velocity shown in the lower left panel of 14. I also used more frequencies than in the previous migration. The new migration stack is shown in Figure 16. Some reflectors stack better in the newer result, and amplitude anomalies are also more consistent.

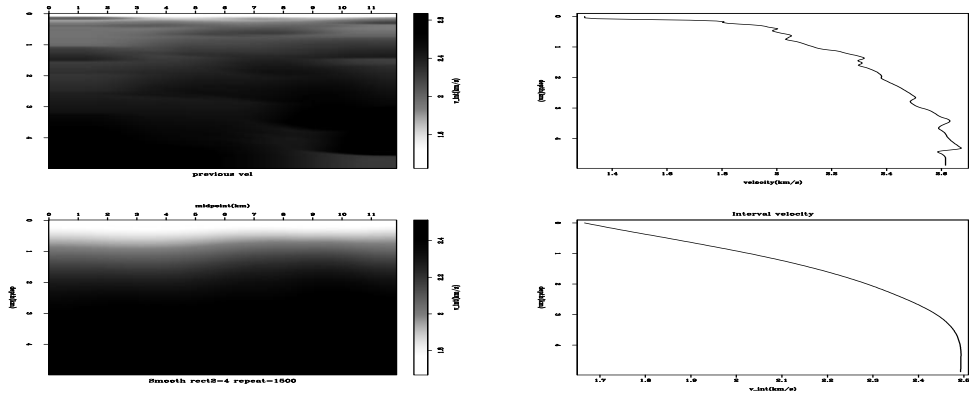

Figure 14: Upper left: previous interval velocity model. Upper right: v(z) model constructed by smoothing it many times. Lower left: new interval velocity model for migration. Lower right: "v(z)" profile constructed by smoothing the new velocity model across midpoint nick2-veloplot [CR]

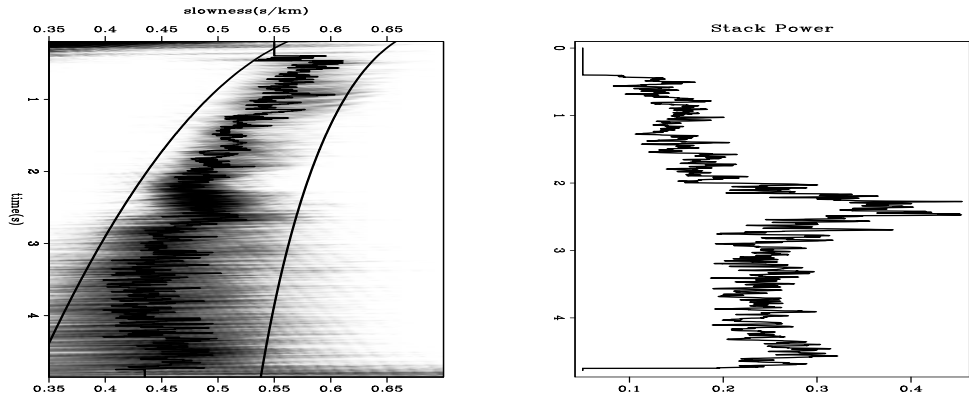

Figure 15: Illustration of the velocity analysis for one midpoint: autopicker fairway, automatic picks, and inversion weights. nick2-phw [CR]

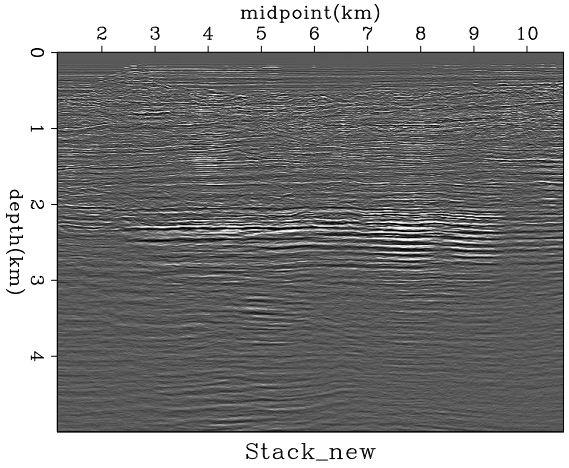

Figure 16: New migrated stack nick2-kaer_new [CR]